ELSEVIER

Nuclear Instruments and Methods in Physics Research A 488 (2002) 419–427

NUCLEAR INSTRUMENTS & METHODS IN PHYSICS RESEARCH Section A

www.elsevier.com/locate/nima

Refraction contrast in X-ray imaging

J. Keyriläinen*, M. Fernández, P. Suortti

Department of Physics, University of Helsinki, P.O. Box 64, FIN-00014 Helsinki, Finland

Received 5 November 2001; received in revised form 11 January 2002; accepted 14 January 2002

Abstract

A two-crystal diffractometer in the non-dispersive configuration is used for measurement of the effects of refraction in weakly absorbing test objects. Characteristic $K\alpha_1$ radiation from a fine-focus X-ray tube with Mo anode is used. The probing beam is about 70 μm wide and 3 mm high. The sample is placed between the monochromator and analyzer, and it is scanned through the beam. The analyzer is tuned to reflect at the low-angle slope, at the top, or at the high-angle slope of the rocking curve, when the sample is not in the beam. Refraction changes the angle of incidence on the analyzer causing changes in intensity. The observed intensity distributions are exactly reproduced by a calculation, where only the effects of refraction are included. The effects of in-beam interference are negligible or very small, which is also verified by changing the distance between the object and the detector.

PACS: 41.50.+h; 42.25.Gy; 87.59.−e; 07.85.Qe

Keywords: X-ray refractive index; Diffraction-enhanced imaging; Two-crystal diffractometer

1. Introduction

New medical imaging techniques have been introduced in the last few decades, and the methods are continuously improved. The relative merits of the techniques depend on the response of the target or its function, which gives rise to the contrast, and on the spatial and temporal resolution. Another important aspect is the radiation dose, which is the limiting factor in those techniques where ionizing radiation is used. X-rays were the first probe of the inner body, and still the most widely used modality of medical imaging is based on the use of X-rays. Their advantages are the availability and good spatial resolution. On the other hand, clinical X-ray imaging is based on differences in absorption, and the contrast is modest when soft tissues are imaged. One of the most important recent applications of X-ray imaging is mammography. Extensive screening programs have been introduced in many countries, and millions of mammograms are taken each year. However, the results are often inconclusive, and false-positive and even false-negative findings are common. The main reason is that the absorption contrast is low, because the variations of elemental composition and density are small, except in micro-calcifications.

It is well known that the density variations of the object cause changes in the phase of the X-ray

*Corresponding author. Tel.: +358-9-1915-0628; fax: +358-9-1915-0639.

E-mail address: jani.keyrilainen@helsinki.fi (J. Keyriläinen).

0168-9002/02/$ - see front matter
PII: S0168-9002(02)00442-4

wave, and when the object is composed of light elements the relative changes in the phase are orders of magnitude larger than the changes in the amplitude of the wave. However, the effects of the phase change become visible only by interference with a reference wave, and this requires development of new imaging methods. The phase change is described by the change in the real part of the refractive index of X-rays. When there is a local gradient of the refractive index in the direction perpendicular to the incident wave vector, there is a change in the wave front. The change, both in the phase and the propagation direction, can be observed using the reflection of a perfect crystal, or directly in the transmitted intensity, if the incident beam is sufficiently coherent. The experimental methods include X-ray interferometry, in-beam holography, and analysis of the refraction angle [1–5].

It is evident that the contrast observed by using a perfect crystal analyzer includes contributions from the interference of the forward-scattered wave with the unscattered wave, change in the propagation direction, and phase changes of the analyzer itself. Different interpretations have been given, and the contrast arising from changes in the wave front has been demonstrated in several experiments [6–8]. When synchrotron radiation reflected from a narrow-band monochromator is used, the degree of coherence is high both longitudinally and transversely, and phase contrast is observed even without a crystal analyzer [9]. When an extended X-ray beam and an area detector are used with an analyzer, the effects of the in-beam interference and changes in the propagation direction are not separated. For this reason, it was decided to make systematic studies of the contrast formation in objects with well-defined density gradients using a narrow, monochromatic X-ray beam from a conventional source.

2. Refractive index and contrast

The spatial contrast arises from variations in the charge density of the object, $\rho(\mathbf{r})$. The effects on the propagation of the X-ray wave can be conveniently described by the refractive index n, which is a complex quantity [10]:

$$n = 1 - \delta - \mathrm{i}\beta. \tag{1}$$

The real part δ corresponds to the phase shift due to scattering, and the imaginary part β to absorption of the wave. It is important that at short wavelengths $n<1$, which gives rise to the total reflection of X-rays at a grazing incidence on a denser medium. The real and imaginary parts can be written in terms of the atomic scattering factor, $f = f_0(\theta) + f' + \mathrm{i}f''$:

$$\delta = [r_e\lambda^2/2\pi]\sum_k N_k(Z_k + f_k') = \left[r_e hc/2\pi E^2\right]\sum_k N_k(Z_k + f_k') \tag{2a}$$

$$\beta = \left[r_e\lambda^2/2\pi\right]\sum_k N_k f_k'' = [hc/4\pi E]\,\mu(E). \tag{2b}$$

Here 2θ is the scattering angle, $r_e = e_2/mc^2 = 2.818\times10^{-15}$ m, the electron classical radius, λ the X-ray wavelength, N_k the number of atoms per unit volume, $Z_k = f_{0k}(0)$ the atomic number, h the Planck constant, c the velocity of light, and $\mu(E)$ the linear absorption coefficient at photon energy E. It is seen that the real and imaginary parts have very different dependencies on the photon energy; in the regime where the photoelectric effect dominates $\beta\propto E^{-4}$, while $\delta\propto E^{-2}$ except in the vicinities of absorption edges. Over a distance z, the intensity of the X-ray beam is attenuated by a factor $\exp(-\langle\mu\rangle z)$, where

$$\langle\mu\rangle z = (4\pi/\lambda)\int \beta\,\mathrm{d}z \tag{3a}$$

and the phase of the wave changes by

$$\phi = (2\pi/\lambda)\int \delta\,\mathrm{d}z = r_e\lambda\rho(x,y) \tag{3b}$$

where $\rho(x,y)$ is the projected electron density on the plane perpendicular to the beam.

For the present experiments, it is essential that the real part of the refractive index dominates contrast formation. MoKα_1 radiation ($\lambda = 0.07093$ nm, $E = 17.48$ keV) is used, and the test objects are made of acrylic, $(C_5H_8O_2)_n$, nylon $(C_{12}H_{22}O_3N_2)_n$, or glass (borosilicate). The density of acrylic is $\rho = 1.20\,\mathrm{g\,cm^{-3}}$, and the linear absorption coefficient for MoKα_1 radiation is

Table 1
Dimensions of the samples and parameters used for calculation of the refraction angles

Sample	Diameter (mm)	ρ (g cm^{-3})	Z/A	$\delta \times 10^6$	μ/ρ (cm^2 g^{-1})
Air		1.29×10^{-3}	0.4992	0.001	1.20
Acrylic (PMMA)	10.00	1.20	0.5394	0.879	0.73[a]
Nylon (PA6)	0.31	1.13	0.5448	0.836	0.736
Glass (borosilicate)	1.76 (o) 1.28 (i)	2.23	0.4971	1.506	5.00[a]

[a] The absorption coefficient is calculated from the measured attenuation at the center of the object.
(o) indicates the outer diameter of the capillary, and (i) indicates the inner diameter.

0.88 cm^{-1}. Other values are given in Table 1. For a numerical calculation of the phase change, it is useful to introduce an approximation of the real part:

$$\delta = 2.70 \times 10^{10}\,(Z/A)\rho[\mathrm{g\,cm^{-3}}]\,\lambda^2[\mathrm{cm^2}] \approx 1.35 \times 10^{10}\rho\lambda^2. \quad (4)$$

In the case of acrylic, the absorption thickness is $t_a = 1/\mu = 11.4$ mm, whereas the phase thickness with $t_p = \lambda/\delta = 86\,\mu$m is more than two orders of magnitude smaller.

The observed interference pattern depends on the degree of coherence of the incident X-ray beam. For each individual wavelet, there is interference between the scattered spherical wave and the unscattered plane wave, but for a visible effect, a coherent superposition within a sufficiently large volume is needed. The longitudinal or temporal coherence is proportional to the monochromaticity of the beam, and the coherence length is defined as $l_c = \lambda(\lambda/\Delta\lambda)$. The transverse or spatial coherence is determined by the emittance of the source, and the opening angle σ' of the cone of the coherent wave front is defined by $\sigma\sigma' = \lambda/4\pi$, where σ is the diameter of the source. The contrast or variation of intensity on the image plane is proportional to the second derivative of the projected electron density, i.e. contrast at edges is enhanced [3]. It is not necessary for the whole object or field of view to be coherently illuminated, but it is sufficient that transverse coherence prevails over an area where appreciable changes in $\rho(x, y)$ take place. On the other hand, the geometrical features of the contrast are independent of the wavelength, i.e. longitudinal coherence of the incident beam is not essential.

A new dimension is added to the contrast formation when the transmitted beam is analyzed by a perfect crystal. The crystal acts as a very narrow angular slit, the width being typically a few μrad only. The experimental arrangements are based on the so-called non-dispersive setting, where the angular broadening due to the finite wavelength band and beam divergence is eliminated. When the object is placed in the beam between the monochromator and the analyzer, the propagation direction changes due to refraction, and the working point on the analyzer rocking curve changes accordingly. The distribution of phases within the reflected beam is changed as well, because there is a phase shift of 180° across the reflectivity curve of the analyzer. The observed contrast depends on the transverse coherence of the beam and on the resolution of the detector, i.e. on the relevant length scales of the experiment. It has been suggested that refraction effects and interference effects at edges can be distinguished, the former giving rise to 'area contrast' and the latter to 'boundary contrast' [6]. It is true that no transverse coherence of the incident beam is needed for the refraction effects, whereas a minimum degree of transverse coherence is required for interference. However, it turns out that appreciable refraction contrast is seen only when $\rho(x, y)$ changes strongly, so that the effects of refraction and interference are superimposed.

The aim of the present experiment is to study contrast formation in length scales that are relevant in mammography. The resolution of X-ray films is in the μm range, but changes in

$\rho(\mathbf{r})$ are seen with sufficient contrast only in the 10–100 μm range. Diffraction-enhanced imaging (DEI) is a new method, which is based on the refraction contrast, and the typical resolution is about 100 μm [5]. The experiments have been carried out at synchrotron sources using narrow-band monochromators, so that the X-ray beam has a high degree of coherence in the relevant object volumes, and the effects of refraction and interference co-exist. For a better understanding of the relative importance of these effects, an experimental setup with essentially incoherent radiation is used, so that only the effects of refraction should be seen. These have been demonstrated by a synchrotron radiation experiment using wedges, so that the interference effects at edges were not recorded [8]. In the present experiment, different cylindrical objects are used, so that pronounced edge contrast is expected. The experimental results are compared with the calculated intensity of the transmitted beam.

3. Experimental setup

The experiment was designed for quantitative studies of the refraction contrast in well-characterized test objects. A narrow X-ray beam is reflected from a perfect Si crystal monochromator, the sample is scanned through the beam, the transmitted beam is reflected by the analyzer, and the intensity is recorded by a low-noise detector. The layout of the experiment is shown in Fig. 1. A fine-focus sealed X-ray tube with Mo anode was used. The take-off angle was 1.32°, so that the apparent width of the 0.4 mm wide line focus was 9.2 μm. The height of the source was limited to 3 mm by a slit at the tube window. Another slit was placed at the end of a beam pipe, 1588 mm from the source. The height of the slit was usually 3 mm, and the width could be adjusted between 20 μm and 1 mm. The beam was reflected by Si($h\,h\,h$) crystals, which were strain-free mounted on goniometer heads. The 111 reflection was used for alignment, and great care was exercised to ensure that the tube focus and the collimating slit were vertical, and that the beam path was in the horizontal plane. The 333 reflection from the monochromator and analyzer was used in the measurements. The two-crystal rocking curve $R(\varepsilon)$ in the non-dispersive setting is shown in Fig. 2 together with the calculated curve; here ε is the rocking angle relative to the nominal Bragg angle θ_B. The width of the rocking curve is very sensitive to the tilt angle of the second crystal. The width was minimized by manual adjustment of the goniometer head, but still the experimental curve is slightly wider due to the vertical divergences of the beam and residual deviations of the scattering vectors from the horizontal plane [11]. Furthermore, the effects of high-frequency vibrations may not be excluded. The fine rotation of the analyzer crystal was effected by special attachments of the goniometer [12]. The resolution and read-out precision of this torsion/bending device is about 1 nrad. A NaI(Tl) scintillation detector

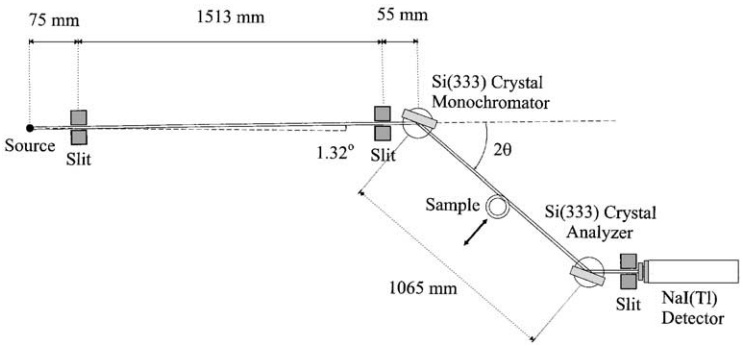

Fig. 1. Experimental setup for refraction contrast studies. The source is a sealed-off X-ray tube with Mo anode. The optical width of the tube focus is 9.2 μm, and the width of the collimating slit is 50 μm. The sample is scanned across the beam in steps of 1 μm.

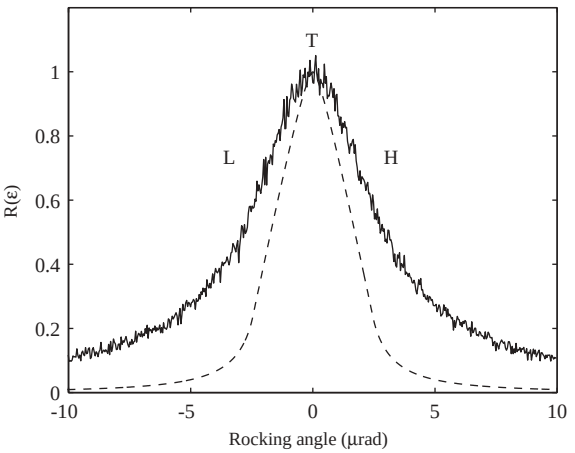

Fig. 2. Experimental (solid line) and calculated (broken line) double-crystal rocking curves of the Si(3 3 3) reflection with MoKα_1 radiation. Background has not been subtracted from the experimental curve. The low-angle, top, and high-angle positions on the rocking curve are indicated by L, T, and H, respectively.

with pulse height discrimination was used for photon counting.

The test objects were acrylic rods, nylon wires and glass capillaries. They were mounted vertically on a high-resolution translation table and scanned through the beam. The horizontal intensity profile of the beam was determined by scanning a vertical knife-edge across the beam. The intensity profile is nearly Gaussian with a FWHM of 70 or 80 μm, depending on the distance from the source, and these values agree closely with the values calculated from the width of the tube focus and that of the collimating slit. The diameter and density of the acrylic rods were measured, and those for the nylon wire and glass capillaries were estimated from tabulated values and from X-ray radiographs. The numerical values are collected in Table 1.

Data acquisition and the motions of the motors driving the analyzer rotation and the sample stage were controlled by a software called SPEC [13]. In the beginning of each measurement, the analyzer was tuned without the sample to reflect at the top (T) of the rocking curve or at the middle of the slope on the low (L) or high (H) angle side of the rocking curve. When the sample is inserted in

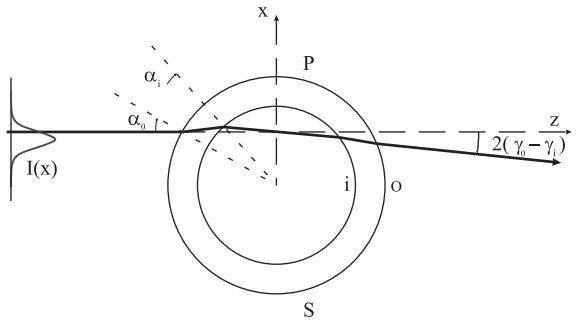

Fig. 3. Refraction of a narrow ray at a capillary. The intensity distribution of the incident beam is indicated by $I(x)$, and the incident angles at the outer and inner surfaces by α_o and α_i, respectively. P indicates the port side and S the starboard side of the sample, and i and o the inner and outer surfaces, respectively.

the beam, the propagation direction changes, and the angle of incidence on the analyzer changes. The working point moves along the rocking curve translating the refraction angle to a change in intensity. Refraction in a cylindrical object is illustrated in Fig. 3. The refraction angle γ can be calculated from Snell's law:

$$\gamma = (\delta_2 - \delta_1)\tan\alpha, \tag{5}$$

where α is the angle of incidence. When the normal of the surface is perpendicular to the direction of the incident beam, this expression diverges, so that care must be exercised in numerical calculations. The lateral shift of the beam due to refraction is very small, so that the deflection angle is 2γ. In the case of a capillary, the refraction angles at the inner surface (i) are opposite to the refraction angles at the outer surface (o), and the total refraction angle is $2\gamma = 2(\gamma_o - \gamma_i)$. It is evident that for a solid rod the angle of incidence at the analyzer decreases ($\gamma < 0$) at the port (P) side of the object and increases ($\gamma > 0$) at the starboard (S) side, moving the operation point to lower or higher angles, respectively. At the T-position of the analyzer, the intensity decreases on both sides, whereas an increase is seen in the (P, H) and (S, L) situations, and a decrease in the (P, L) and (S, H) situations, if $|\gamma|$ is sufficiently small. The directions are reversed at the inner edges of a capillary, and the net effects are not evident without a detailed calculation.

The interference contrast at the edges, where $\partial^2\rho(x)/\partial x^2$ is large, increases with the distance between the object and the detector [3]. The transverse coherence length is only of the order of 1 μm in the present arrangement where the beam is not magnified by an asymmetric reflection, and therefore the interference contrast is expected to be small. Nevertheless, two distances (about 50 and 80 cm) were used between the sample and the detector.

4. Results and discussion

Some of the experimental intensity curves are shown in Figs. 4–6. The importance of the effects of refraction in comparison with those of absorption is most obvious in the case of the thin nylon wire (Fig. 4). The maximum effect of absorption at the center of the wire is 3%, whereas refraction at the edges of the wire changes the intensity reflected by the analyzer by 30–50%. This is an impressive demonstration of the potential of the DEI method in imaging of weakly absorbing objects such as soft tissues. When the analyzer is tuned to the T position, refraction makes the working point to slide down on either side of the rocking curve. The distance between the minima is close to the diameter of the wire. The edge effects are most prominent in the case of the acrylic rod of 10 mm diameter. At the T position, the intensity drops to 10% of the incident intensity when the edge intercepts the beam, whereas the maximum absorption at the middle of the rod is about 60%. The strange-looking behavior at the L and H

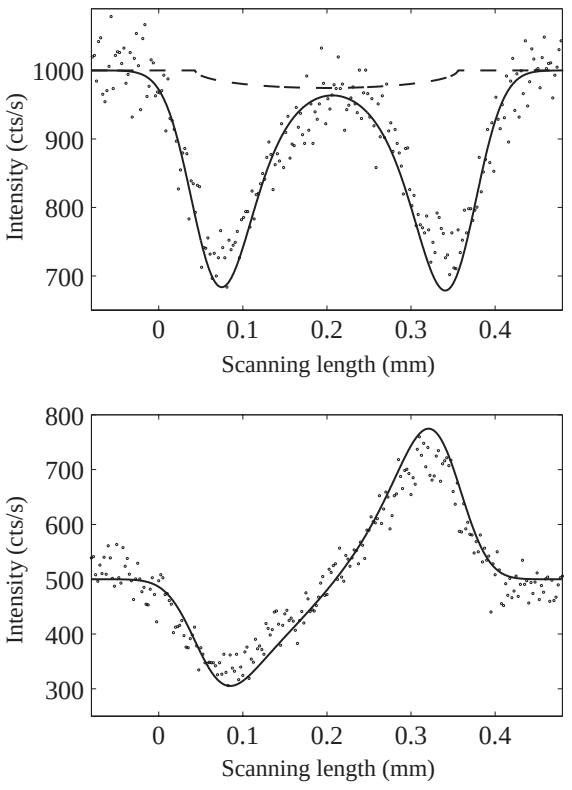

Fig. 4. Nylon wire of 0.31 mm diameter: experimental (points) and calculated (solid line) intensities as reflected by the analyzer crystal at the top (T) position (top) and low-angle (L) position (bottom). The effect of absorption is indicated by the broken line. The scan direction is from P to S.

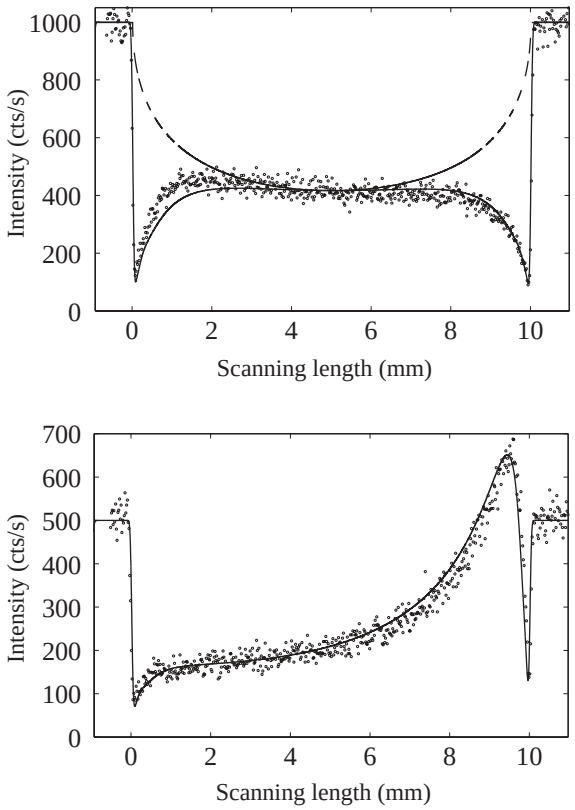

Fig. 5. Acrylic rod of 10 mm diameter: intensities at T position (top) and L position (bottom); cf. Fig. 4.

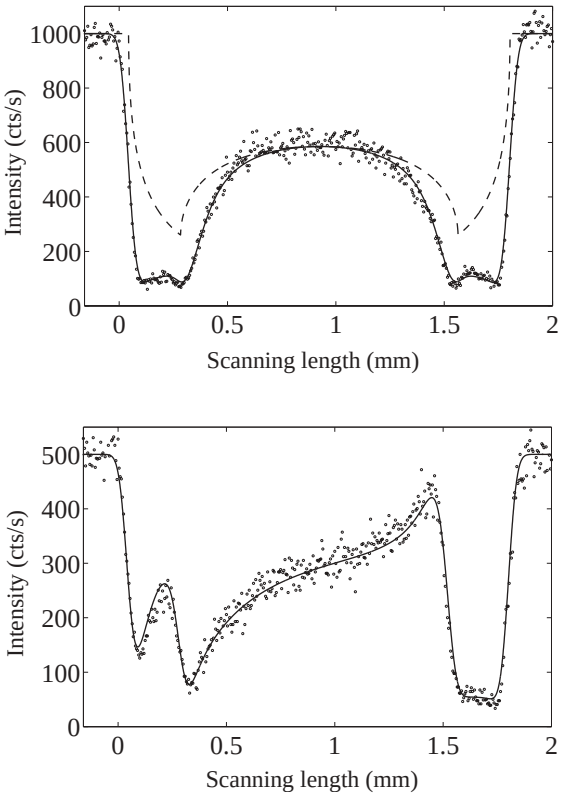

Fig. 6. Glass capillary of 1.76 mm outer diameter and 1.28 mm inner diameter: intensities at T position (top) and H position (bottom); cf. Fig. 4.

positions is explained as follows. Starting at the S edge, strong refraction drives the working point over the T position to the other side of the rocking curve, from L to the opposite tail beyond H (or at the P edge from H beyond L). When the beam moves further into the object, the refraction angle $|\gamma|$ decreases, and the working point begins to climb towards the top of the rocking curve. This happens within a very small distance, and the top is reached at about 0.5 mm from the edge, where absorption decreases the intensity by 30%. Then the working point starts sliding down the slope to L (or H), which is reached at the middle of the rod (the refraction angle is zero). Absorption reduces the intensity by 60% in the same way as at the T position. On the other side of the rod, the refraction angle changes sign, and the working point slides further down along the rocking curve. When the edge is reached, there is again a large drop of intensity, because the working point moves far to the tail of the rocking curve.

In the case of the glass capillary, the effects of refraction are more complicated as four edges are crossed. The outer diameter is 1.76 mm, and the wall thickness about 0.24 mm. The effects of absorption are largest at the inner edges, and in general, the effects of refraction and absorption are combined, so that the intensity curves need a detailed analysis. For instance, the maximum effect of absorption is 70%, but the lowest intensity values are $<10\%$ of the incident intensity near the edges.

The calculated curves are shown together with the experimental results. For a numerical calculation, the intensity distribution $I(x)$ of the X-ray beam was replaced by a histogram of 1 μm wide elements, the refraction angle γ was calculated for each element, $I(x)\,\Delta x$ was multiplied by the transmission factor $\exp(-\mu z)$ and by the reflectivity $R(\varepsilon + 2\gamma)$, and the intensities of the reflected elemental rays were added up. A smoothed experimental reflectivity curve $R(\varepsilon)$ was used, and the absorption coefficients are given in Table 1. The differences between the experiment and the calculation are mostly within the statistical variations of the intensity measurement demonstrating that the contrast is due to refraction at least when the transverse coherence of the incident beam is low. The absorption contrast is shown for comparison, and it is evident that refraction provides a large enhancement of contrast at the edges of the object. The changes in the refraction angle are larger than the FWHM of the rocking curve width of the analyzer. The good agreement between the experiment and calculation demonstrates that the formation of refraction contrast is understood quantitatively.

In the above examples, the change in density at the edge of the object is very large in comparison with density variations of soft tissues. In DEI imaging of soft tissues, the refraction angles at the edges are typically only fractions of μrad, so that the working point moves only slightly on the rocking curve. Still the changes in intensity may be several tens of per cent, when the working point is on the slope of the rocking curve. Near the top of the rocking curve, the intensity changes are small

unless small-angle scattering (SAXS) from the object is strong. In such a case, the analyzer rejects a large fraction of the transmitted beam, and the so-called extinction contrast is observed [8].

Most of the earlier demonstrations of enhanced edge contrast have been qualitative, because extended beams and high-resolution film as the detector have been used. It is interesting to compare the present results with those from an experiment where the refraction angle and intensity changes of a narrow beam were measured with a position-sensitive detector [14]. No analyzing crystal was used, and the observed contrast at the edges of a glass capillary was satisfactorily explained by re-distribution of intensity due to refraction. No provision for interference effects was made, although a partly coherent monochromatic synchrotron beam was used.

The effects of in-beam interference depend on the distance D between the sample and the detector. The optimum contrast due to Fresnel diffraction is observed when the object size is about $(\lambda D)^{1/2}$, and the distances in the present case correspond to 6 and 8 μm [9]. The beam is transversely coherent over about 1 μm only, so that the interference effects are expected to be negligible. Nevertheless, results at two distances are compared in Fig. 7. The density gradient is largest at the edges of the glass capillary. The range where the largest effects of interference contrast are expected are shown in an enlarged scale. There is no discernible difference between the curves, probably because the difference in D is small, but in very narrow ranges near the edges, the experimental curves have sharp minima, which may arise from interference contrast.

The present results give confidence in interpreting the contrast in the DEI method in terms of refraction at the density gradients of the object. The effects of refraction are actually evident in tissue samples when the images taken at the opposite slopes of the rocking curve of the analyzer are compared. The density gradients in these samples are small, but the effects of refraction can be emphasized by subtracting the L-image from the H-image [5].

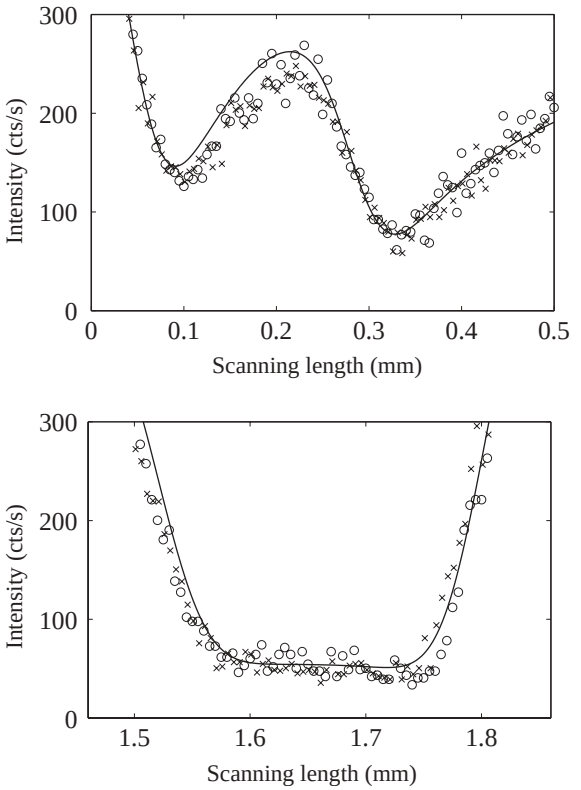

Fig. 7. Enlargements of the regions of minima in Fig. 6. The experimental results correspond to the sample–detector distances of 800 mm (circles) and 500 mm (crosses). The solid line is the calculated curve for the 800 mm distance.

Acknowledgements

The authors thank A. Bravin, S. Fiedler, and W. Thomlinson for discussions and many suggestions for improvements of the experiment, A. Kangasmäki for help in computations, and P. Pihkala for constructing the diffractometer. The financial support from the Academy of Finland is gratefully acknowledged (project no. 162907).

References

[1] U. Bonse, M. Hart, Appl. Phys. Lett. 7 (1965) 99.
[2] A. Momose, Nucl. Instr. and Meth. A 352 (1995) 622.
[3] A. Pogany, D. Gao, S.W. Wilkins, Rev. Sci. Instrum. 68 (1997) 2774.

[4] V.A. Bashuev, V.N. Ingal, E.A. Beliaevskaya, Crystallogr. Rep. 41 (1996) 766.
[5] D. Chapman, W. Thomlinson, R.E. Johnston, D. Washburn, E. Pisano, N. Gmür, Z. Zhong, R. Menk, F. Arfelli, D. Sayers, Phys. Med. Biol. 42 (1997) 2015.
[6] V.N. Ingal, E.A. Beliaevskaya, J. Phys. D 28 (1995) 2314.
[7] T.J. Davis, T.E. Gureyev, D. Gao, A.W. Stevenson, S.W. Wilkins, Phys. Rev. Lett. 74 (1995) 3173.
[8] Z. Zhong, W. Thomlinson, D. Chapman, D. Sayers, Nucl. Instr. and Meth. A 450 (2000) 556.
[9] A. Snigirev, I. Snigireva, V. Kohn, S. Kuznetsov, S. Schelekov, Rev. Sci. Instrum. 66 (1995) 5486.
[10] R.W. James, The Optical Principles of the Diffraction of X-rays, G. Bell and Sons Ltd., London, 1962.
[11] M.M. Schwarzchild, Phys. Rev. 31 (1928) 162.
[12] P. Suortti, J. Keyriläinen, M. Fernández, unpublished.
[13] SPEC, software product by Certified Scientific Software (www.certif.com).
[14] N. Yagi, Y. Suzuki, K. Umetani, Y. Kohmura, K. Yamasaki, Med. Phys. 26 (1999) 2190.